# Graph-based retrospective 4D Image construction from free-breathing MRI slice acquisitions

Yubing Tong[1], Jayaram K.Udupa[1], Krzysztof C. Ciesielski[1,2], Joseph M. McDonough[3], Andrew Mong[3], Robert M. Campbell[3]

[1]Medical Image Processing Group, Department of Radiology, University of Pennsylvania, Philadelphia, PA, 19104

[2]Department of Mathematics, West Virginia University, Morgantown, WV, 26505

[3]Center for Thoracic Insufficiency Syndrome, Children's Hospital of Philadelphia, Philadelphia, PA, 19104

## ABSTRACT

4D or dynamic imaging of the thorax has many potential applications [1, 2]. CT and MRI offer sufficient speed to acquire motion information via 4D imaging. However they have different constraints and requirements. For both modalities both prospective and retrospective respiratory gating and tracking techniques have been developed [3, 4]. For pediatric imaging, x-ray radiation becomes a primary concern and MRI remains as the de facto choice. The pediatric subjects we deal with often suffer from extreme malformations of their chest wall, diaphragm, and/or spine, as such patient cooperation needed by some of the gating and tracking techniques are difficult to realize without causing patient discomfort. Moreover, we are interested in the mechanical function of their thorax in its natural form in tidal breathing. Therefore free-breathing MRI acquisition is the ideal modality of imaging for these patients. In our set up, for each coronal (or sagittal) slice position, slice images are acquired at a rate of about 200-300 ms/slice over several natural breathing cycles. This produces typically several thousands of slices which contain both the anatomic and dynamic information. However, it is not trivial to form a consistent and well defined 4D volume from these data. In this paper, we present a novel graph-based combinatorial optimization solution for constructing the best possible 4D scene from such data entirely in the digital domain. Our proposed method is purely image-based and does not need breath holding or any external surrogates or instruments to record respiratory motion or tidal volume. Both adult and children patients' data are used to illustrate the performance of the proposed method. Experimental results show that the reconstructed 4D scenes are smooth and consistent spatially and temporally, agreeing with known shape and motion of the lungs.

**Key words:** Dynamic MR imaging, 4D image construction, graph optimization, imaging lungs

## 1. INTRODUCTION

Dynamic imaging and 4D image construction of the thorax are extremely useful tools in the study, diagnosis, treatment, and management of numerous diseases of the thorax, lungs, rib cage, and the diaphragm. Among medical imaging modalities, CT and MRI offer sufficient speed to acquire motion information via dynamic (or 4D) imaging of the thorax. 4D-CT involves additional radiation dose over and above the level associated with static imaging, which, especially for pediatric subjects, becomes difficult to justify. Furthermore, this modality does not provide sufficient information about soft-tissue components which are the primary focus in some disease conditions [5]. On the other hand, MRI has excellent soft-tissue contrast and imposes no radiation hazard. In addition, the pediatric subjects we deal with in our imaging application area often suffer from extreme malformations of their chest wall, diaphragm, and/or spine, as such patient cooperation needed by some of the gating and tracking techniques in 4D CT imaging are difficult to comply with without causing patient discomfort. Since we are interested in the mechanical function of the thorax of these patients in its natural form in tidal breathing, free-breathing MRI acquisition is the ideal modality of imaging for these patients.

4D MRI approaches may be grouped into two categories: those using fast 3D MRI sequences to acquire pseudo real-time volumetric images [6, 7] and those using fast 2D MRI sequences to continuously acquire images from all respiratory phases and then retrospectively sort those images by respiratory signal [8-13]. It is almost impossible for the first

approach to acquire high resolution 4D images without significantly compromising image quality. The second approach requires some form of respiratory surrogate (internal or external) signal to capture respiratory phase information, which is then used to monitor patient motion during image acquisition. Compared with the first approach, the image quality of the second method is usually superior and voxel size is smaller with increased in-plane spatial resolution. Our proposed approach may be classified as belonging to the second group with one important difference in that it neither tracks nor uses a surrogate signal to identify respiratory phases of the acquired slices.

Instead of using external respiratory signal or extracting respiratory signal first from images and then use it to sort CT/MR images as done in manifold learning techniques [8-11], we propose a direct solution for 4D MR image construction that is simple and practical. The idea is to group, for each respiratory phase, the most similar slice images (with high similarity in space and intensity) to construct the best spatial 3D volume; then to group the spatial 3D volumes into the best respiratory period to construct a 4D image by searching all 3D volumes. Graph-based path optimization algorithms are employed selecting the best grouping. Constructed 4D images are evaluated by checking the degree of smoothness of every 3D volume and volume consistency between adjacent time instances and periodicity over the selected best respiratory period.

The paper is organized as follows. The 4D MR image construction method is described in Section 2. Evaluation, experiments, and results are presented in Sections 3, and Section 4 summarizes our conclusions.

## 2. 4D IMAGE CONSTRUCTION METHOD

An ideal 4D image $B$ of a body region (such as the thorax) of a patient, is considered to be a time sequence $B(t)$, where a time marker $t$ varies over a time interval $[0, \tau]$. For a fixed time instance $t \in [0, \tau]$, ideal image $B(t)$ is interpreted as a 3D image, that is, as an intensity function defined on a fixed rectangular domain $\Omega = X \times Y \times Z \, mm^3$. We assume that $\Omega$ is defined with respect to an imaging device $xyz$ coordinate system, called the *scanner coordinate system, SCS*, which is expressed in millimeters. The data provided by the imaging device is treated as samplings of this idealized 4D image. Our goal is to use this data to approximate $B(t)$ for $t$ varying over one full breathing cycle.

There are dynamic imaging schemes which currently acquire images while the patient is freely breathing. The data they produce is in the form of a sequence $A = \{ f_1, \ldots , f_M \}$ of 2D images, each 2D image being a slice of $B$ for a fixed value $z \in Z$ and a time instance $t \in [0, \tau]$, that is, $f_i$ is a 2D image defined on $X \times Y$ and $f_i(x, y)$ is the intensity of $B$ at (x, y, z) at the time instance $t_i$ of acquisition. Each slice image $f_i$ is acquired within a very short time interval such that the motion may be thought of as being frozen during that time. For each fixed $z$-position in SCS, slice acquisitions are made in this manner over several breathing cycles and the process is moved to the next $z$-position, etc. The number of $z$-locations where the acquisition takes place, as well as the actual $z$-coordinates of these locations, are known in this scheme. In what follows, we will denote them as $z_1,...,z_K$ and treat $Z$ as equal to $\{z_1,...,z_K\}$.

The acquisition scheme can be graphically depicted as shown in Figure 1, where the line at the top of the figure indicates continuous timeline from start to end of scan, and each time interval demarcated by a successive pair of vertical line segments indicates the time duration over which slice acquisitions (denoted by dots) are made for each $z$-location $z_i$. The lower portion of Figure 1 is a graphical representation that will be used in our method. In this representation, the time interval corresponding to each $z$-location $z_i$ is expanded and drawn as a horizontal dotted line. Each bold dot on this line represents an acquired slice image.

The actual motion of $B(t)$ may be thought of as being quasi-periodic in the following sense. Consider the thorax and the breathing motion for example. Although it is a repetitive process, it cannot be usually considered to be perfectly periodic. The patient may take a shallow versus a deeper breath, although we will rule out more severe disturbances such as swallowing and coughing. The data are acquired for each $z$-location over a period of time to provide enough slices to describe the motion. This is typically repeated over several breathing cycles. Mathematically, quasi-periodicity can be represented as a mapping $\varphi$ from $[0, \tau]$ into a circle $C$, representing respiratory phase, with the property that for any time instances $t, t' \in [0, \tau]$, if $\varphi(t) = \varphi(t')$ (i.e., the time instances point to the same phase of the breathing cycle), then the 3D images $B(t)$ and $B(t')$ are (approximately) equal. This is the key, since the acquisition schema does not provide us full 3D image $B(t)$ for any time instance $t$; so during the construction process, some sections of the constructed $B(t)$ will actually be the sections of $B(t')$ for another time instance $t'$ of the same (or similar) breathing phase (i.e., $\varphi(t') = \varphi(t)$). More specifically, our output – a digital approximation of one full breathing cycle – will be of the form of a mapping $F$

from $Z \times T$ into 2D images on $X \times Y$, where $T$ is a finite subset (digital approximation) of the phase circle $C$, and, for every $(z, t) \in Z \times T$, $F_{z,t}$ is one of the data images $f_i$ for which $z_i = z$ and $\varphi(t_i) \approx t$, so that the resulting map $F$ leads to the best 4D image representing a breathing cycle.

We choose our solution, a map $F$, in three stages. In *Stage 1*, we associate with each slice $f_i$ an approximate breathing phase $\varphi(t_i) \in C$ at which the slice was taken. We also determine a digital approximation $T$ of $C$ that will be used to express $F$. In *Stage 2*, for each breathing phase $t \in T$ and each slice $f_i$ with $\varphi(t_i) = t$, we find a 3D scene $F_t$ – a mapping from $Z$ with $F_t(z) = F_{z,t} = f_j$, *where* $z_j = z$ *and* $\varphi(t_i) \approx t$ – containing the slice $f_i$ and optimal w.r.t. the criteria described below. These spatial 3D scenes can be combined together to yield several instances of a 4D scene representing a full breathing cycle. In *Stage 3*, we decide which of these instances is to be taken as output. The steps associated with these three stages are described below.
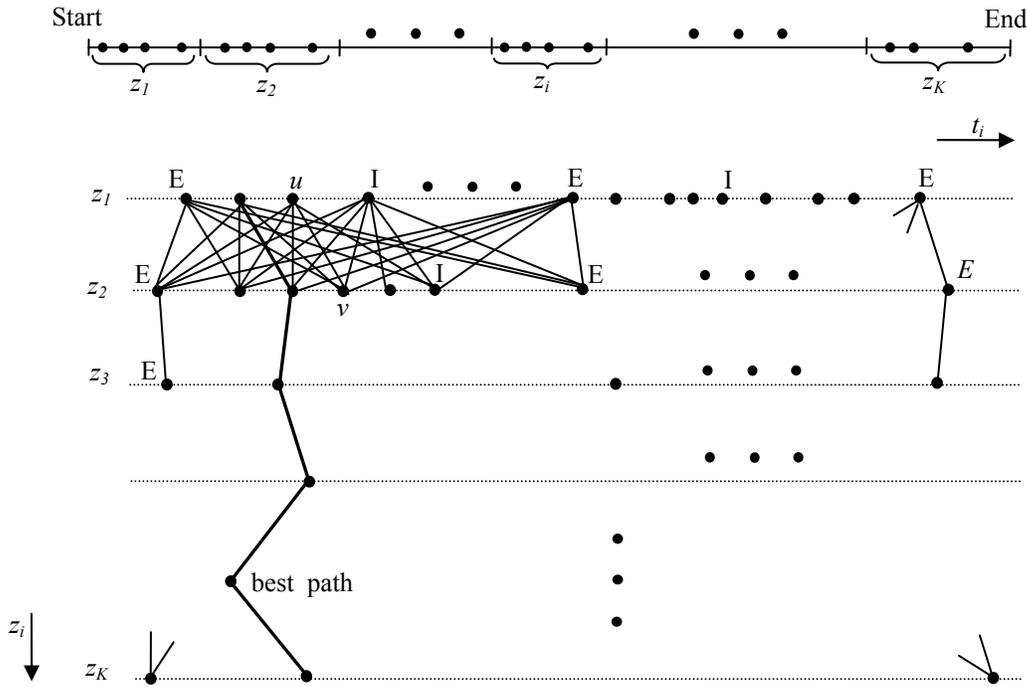


Figure1. Graph built from slices acquired at different time instances and *z*-positions.

## Stage 1 - Determining breathing phases

At each *z*-location along the corresponding horizontal line in Figure 1, we mark each breathing period by visually examining all time slices and identifying slices corresponding to end expiration and end inspiration. Accordingly, the identified slices are marked E and I, respectively. At present this is done manually, by observing the motion of the diaphragm. In the future, this step will be automated. All slices (bold dots or nodes on the horizontal line) lying between a slice labeled E and the next slice labeled E along that line constitute one breathing period. If the slices $f_n, f_{n+1}, \ldots, f_{n+m}$ represents $k$th such period, then we consider these slices as being spread over $m$ equally distributed phases of the breathing cycle. That is, we let $T_k = \tau_0, \ldots, \tau_m$ be the set of equally distributed $m$ points on the circle $C$ (with $\tau_j = \langle\ cos(\dfrac{2\pi j}{m}), sin(\dfrac{2\pi j}{m})\ \rangle$ ) and define $\varphi(t_{n+j}) \approx \tau_j$ for $j \in \{0,\ldots,m\}$. We define $T$ as $T_k$ of the smallest size. Notice that the precision with which this identification is made is not that critical, since best 3D scenes are found by path optimization as we explain below.

**Stage 2 - Determining optimal 3D scenes**

*Building a weighted graph:* A graph $G = (A, P, w)$ is constructed to represent the relationship among the slice images $f_i$ in terms of their potential spatial contiguity, as illustrated in Figure 1. The slices in $A$ form the nodes of the graph and each arc in the set $P$ of arcs/edges (solid lines in Figure 1) represents a pair of slices $\{u, v\}$, where $u$ and $v$ are any slices from two adjacent $z$-locations. Note that the dotted lines in the figure are only for indicating the $z$-locations of the slices and do not represent arcs.

Each arc $e = \{u, v\}$ is given a weight (cost) $w(e)$, also written as $w(u, v)$, to express the unlikeliness of the slices $u$ and $v$ to come from the same time-frozen anatomic volume. The weight consists of the following three components: $w_g(u,v)$ that dependents on the difference in gray intensity of the slices $u$ and $v$, $w_s(u,v)$ that dependents on the sign and $w_p(u,v)$ that dependents on the difference in $z$-positions of the slices $u$ and $v$. These components are combined via formula: $w(u,v) = w_g(u,v) \cdot w_s(u,v) \cdot w_p(u,v)$. Concerning $w_g(u,v)$, rather than using a straightforward root mean squared (RMS) difference between the pixel intensities of slices $u$ and $v$ for determining the value of $w_g(u,v)$, we exploit knowledge of the appearance of the slice images and of the specific objects that move the most in $B(t)$. For example, in the thorax, the base of the lungs moves the most, and, since the lungs typically appear dark in MR images, we weight the changes from $u$ to $v$ from dark to brighter intensities more heavily than other changes. The component $w_s(u,v)$ takes into account the sign of this difference, so the contiguity of the motion is also accounted for. The idea behind $w_p(f_i, f_j)$ is to assign a higher weight whenever the distance between their positions $\varphi(t_i)$ and $\varphi(t_j)$ is larger. That is, if $u = f_i$ and $v = f_j$ are similarly positioned within their respective respiratory periods, then they will be considered 'close' and the weight will be low. The weight will increase with the degree of mismatch in their respiratory phase.

*3D scene construction via optimal path search:* Once the graph $G$ is built, an optimal 3D scene is constructed for each of a selected set of respiratory phases by using Dijkstra's algorithm and searching for an optimal path for each $\mu = f_i$ for which the corresponding breathing period $T_k$ is of the smallest size, that is, $T_k = T$. For each such $\mu = f_i$ we find a path $A_\mu = \left\langle f_{n_1},...,f_{n_K} \right\rangle$ in $G$ such that: each $f_{n_j}$ represents a slice with its $z$-coordinate being $z_j$; the path contains $f_i$, that is, $f_i = f_{n_m}$ for some $m$; both paths $\left\langle f_{n_1},...,f_{n_m} \right\rangle$ and $\left\langle f_{n_m},...,f_{n_K} \right\rangle$ are optimal. We consider each such constructed path $A_\mu$ as a 3D scene for the respiratory phase $\varphi(t_i) \in T$.

**Stage 3 - Constructing an optimal 4D scene**

Consider all sequences $S_k = \left\langle f_n, f_{n+1},..., f_{n+m} \right\rangle$ of slices with the associated breathing cycle set $T_k$ equal to $T$. With each $f_i$ from such $S_k$ we have associated a 3D scene $F_i = A_{f_i}$ found in Stage 2. Then $B^k = \left\langle F_n, F_{n+1},..., F_{n+m} \right\rangle$ is a 4D scene representing one full breathing cycle. We choose one of these 4D images $B^k$, having the smallest cost, as an output of our process. The cost of $B^k = \left\langle F_n, F_{n+1},..., F_{n+m} \right\rangle$ is defined as the mean of the costs of the 3D scenes $F_n, F_{n+1},..., F_{n+m}$, as used in Stage 2.

# 3. RESULTS

## 3.1 Image data

MR image data of the thorax utilized in our evaluation are summarized in Table 1. The data include 9 image sets coming from six subjects. Multiple image sets for the same subject correspond to different patient conditions like pre- and post-surgery. In our set up, for each (coronal or sagittal) slice position, slice images are acquired at a rate of about 200-300 ms/slice over several natural breathing cycles. This produces 1000 – 7700 slices (see table) which contain both the anatomic and dynamic information about the free-breathing thorax.

## 3.2 Results

Qualitative evaluation

All constructed 4D scenes were visualized in both space and time in a cine mode by holding one variable fixed and letting the other change. This allows close scrutiny of the accuracy of 4D construction in terms of the spatial and temporal contiguity of the slices of the 4D scene. Figures 2 and 3 show a static display in this spirit portraying all z-slices corresponding to a fixed time point (Figure 2) and all time-slices for a fixed z-position for one of the test subjects (Adult-1). Spatial contiguity of the slices in Figure 2 and the periodicity of the motion of the dynamic structures is quite evident in these figures. In this example, the constructed optimal 4D scene had spatial dimensions of 192x192x31 and the number of time points was 10. Thus, in this instance, the 4D construction process selected an optimal set of 310 slices over one breathing period from the acquired set of 31x35 = 1085 slices. All 4D constructions of the tested data sets were found to be spatially and temporally contiguous when visualized in this manner in cine mode.

Table 1. Data used in the evaluation of the 4D image construction method.

| Subject | Age | Voxel size (mm$^3$) | Slice size, number of time instances | Number of z-locations | Imaging plane (numbers of scans) |
|---------|-----|---------------------|--------------------------------------|-----------------------|----------------------------------|
| Adult-1 | 30 | 2.21*2.21*4.8 | 192x192, 35 | 31 | coronal (1) |
| Adult-2 | 23 | 2.08x2.08x3.6 | 162x192, 100 | 50 | coronal (1) |
| Child-1 | 9 | 1.17*1.17*6.0 | 224x256, 80 | 35 | sagittal (3) |
| Child-2 | 5 | 1.17x1.07x6.0/ 0.98x0.98x6.0 | 224x256, 80 | 24/45 | sagittal (2) |
| Child-3 | 12 | 1.82x1.82x3.6 | 162x192, 100 | 77 | sagittal (1) |
| Child-4 | 12 | 1.82x1.82x3.6 | 162x192, 100 | 77 | sagittal (1) |
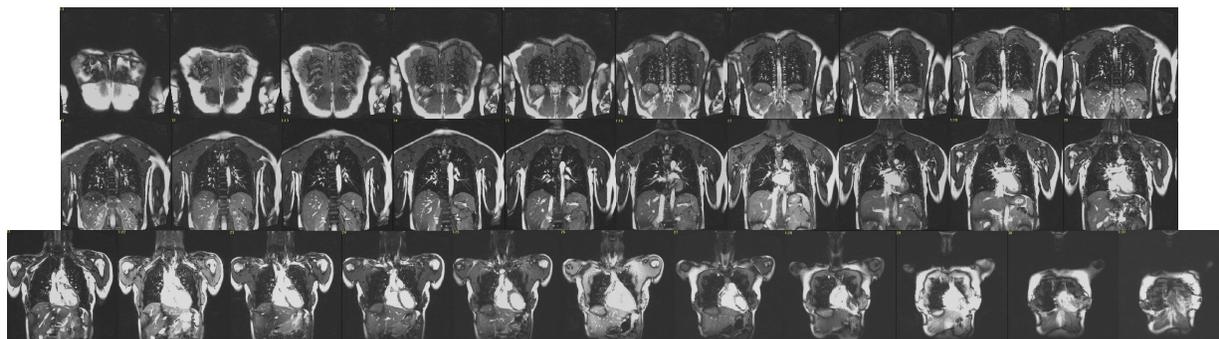


Figure 2. All z-slices constituting a time-frozen spatial volume of the optimal 4D scene constructed from Adult-1 data set. Total 31 slices (from top to bottom, left to right) covering thoracic region from the most frontier to the most posterior scans.
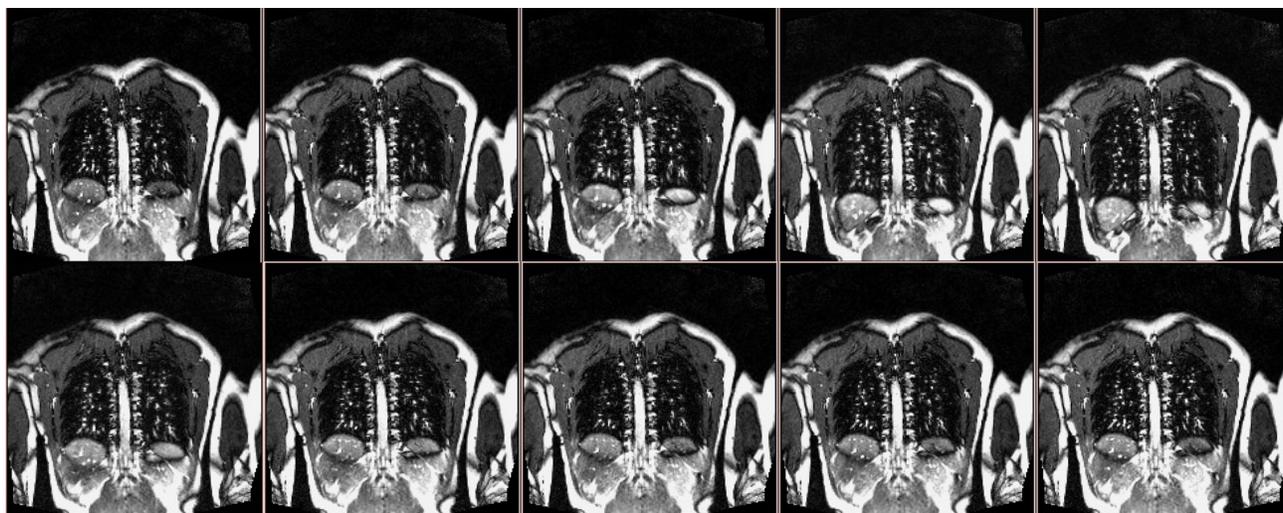


Figure 3. All time-slices over one period from an optimally constructed 4D scene corresponding to a fixed z-location for the data set depicted in Figure 2. Ten time points are included from left to right, top to bottom.

Quantitative evaluation

For both adult subjects, we also collected breath-hold images at end inspiration and end expiration under tidal breathing. These two 3D scenes can be used as ground truth against which the 3D scenes taken at corresponding respiratory phases from the constructed 4D scene, or quantities derived from them, can be compared. One such comparison is shown in Figure 4 for data from Adult-1. The figure plots how the segmented lung area varies over the $z$-slices of the two 3D scenes, on the left for breath-hold image data, and on the right for data derived from the 4D scene. The mean of the areas of the slices over the 3D scene was subtracted for producing these plots. We may observe that the area curves are not only smooth, as can be expected, but also closely resemble the curves for breath-hold images.

As to processing time, the construction algorithm (implemented in MATLAB) takes about 1.5 minutes for all steps on a Dell 2-core 2.8 GHz machine with 3.5 GB of RAM. The main time-consuming step at present is the interactive labeling operation which takes about 20 seconds per $z$-location.
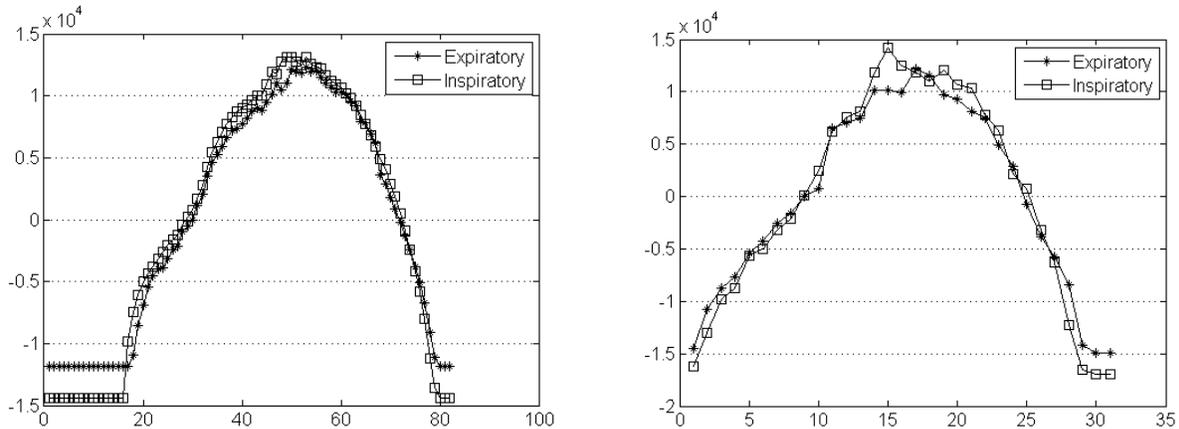


Figure 4. Lung area (vertical axis) on different $z$-slices after subtracting the mean area over all slices. On the left, the curves obtained from the breath-hold data for end inspiration and end expiration are shown. On the right, similar curves derived from the constructed 4D scene are shown. Data pertain to subject named Adult-1 in Table 1.

## 4.  CONCLUSIONS

Imaging the dynamic organs of pediatric subjects and patients is challenging. Dynamic CT is ruled out because of radiation concerns, especially since more data will have to be captured which may increase radiation exposure beyond those of static CT imaging schemes. Any encumbering external device or protocol that may be needed for collecting respiratory signal may be also difficult to work with for this population due to reasons such as not being able to follow instructions or accommodate the instruments, the device interfering with the natural tidal breathing itself, and patients with malformations of the thorax having difficulty in just normal breathing itself. The free-breathing dynamic MRI acquisition protocol utilized in this paper is the only plausible imaging strategy under these circumstances. The proposed method of 4D image construction was arrived at especially for this data collection mode. From our experience so far, the image acquisition method works well with even very sick patients. The proposed 4D construction method is therefore a very practical method of building dynamic image data which are subsequently needed in the analysis of the dynamics of the thorax of these patients, planning treatment, and assessing treatment outcomes.

We provided a preliminary evaluation of the 4D construction method in this paper. More quantitative evaluations are needed to fully establish this method for routine clinical use.

## ACKNOWLEDGEMENTS

## REFERENCES

[1]   Melanie Tory, Niklas Röber, Torsten Möller, Anna Celler, and M. Stella Atkins. "4D Space-Time techniques: A

medical imaging case study," Proc. IEEE Visualization 473-477(2001).

[2] Nehmeh SA, Erdi YE, Pan T, Pevsner A, Rosenzweig KE, Yorke E, Mageras GS, Schoder H, Vernon P, Squire O, Mostafavi H, Larson SM, Humm JL. "Four-dimensional (4D) PET/CT imaging of the thorax," Med Phys 31(12), 3179-86(2004).

[3] Li G, Citrin D, Camphausen K, Mueller B, Burman C, Mychalczak B, Miller RW, Song Y. "Advances in 4D medical imaging and 4D radiation therapy," Technol Cancer Res Treat 7(1), 67-81(2008).

[4] P.J. Keall, S.S.Vedam, R.George.Technical Report, "Respiratory regularity gated 4D CT acquisition: concepts and proof of principle," Australas Phys Eng Sci Med 30(3), 211-20(2007).

[5] G Remmert, J Biederer, F Loherger, M Fabel and G H Hartmann. "Four-dimensional magnetic resonance imaging for the determination of tumour movement and its evaluation using a dynamic porcine lung phantom," Phys Med Bio, 52(18), N401-15(2007).

[6] Cai J, Chang Z, Wang Z, Paul Segars W, Yin FF. "Four-dimensional magnetic resonance imaging (4D-MRI) using image-based respiratory surrogate: a feasibility study," Med Phys 38(12), 6384-94(2011).

[7] Wagshul ME, Sin S, Lipton ML, Shifteh K, Arens R. "Novel retrospective, respiratory-gating method enables 3D, high resolution, dynamic imaging of the upper airway during tidal breathing," Magn Reson Med 70(6), 1580-90(2013).

[8] Wachinger C, Yigitsoy M, Rijkhorst EJ, Navab N. "Manifold learning for image-based breathing gating in ultra-sound and MRI," Med Image Anal 16(4), 806-18(2012).

[9] Manfred.Georg, Richard Souvenir. "Manifold learning for 4D CT Reconstruction of the Lung," CVPRW, (2008).

[10] Manfred Georg, "Simultaneous Data Volume Reconstruction and Pose Estimation from slice samples," CVPR, (2008).

[11] Christian Wachinger, Mehmet Yigitsoy. "Manifold Learning for Image-based Breathing Gating with Application to 4D Ultrasound," MICCAI 13(2), 26-33(2010).

[12] M von Siebenthal, Cattin P, Gamper U, Lomax A, Szekely G. "4D MR imaging using internal respiratory gating," MICCAI 8(2), 336-43(2005).

[13] M von Siebenthal, G Szekely, U Gamper, P Boesiger. "4D MR imaging of respiratory organ motion and its variability," Physics in Medicine and Biology, 52(6), 1547-1564(2007).